Modeling study of $PM_{2.5}$ pollutant transport across cities in China's Jing–Jin–Ji region during a severe haze episode in December 2013

C. Jiang[1*], H. Wang[2*], T. Zhao[1], T. Li[1], H. Che[2]

1 Nanjing University of Information Science & Technology, Nanjing 210044, China
2 Institute of Atmospheric Composition, Chinese Academy of Meteorological Sciences (CAMS), CMA, Beijing, 100081, China

Corresponding author: C.Jiang (jc452@163.com) and H. Wang(wangh@cams.cma.gov.cn)

Abstract

To study the influence of particulate matter (PM) transported from surrounding regions on the high $PM_{2.5}$ pollution levels in Beijing, the GRAPES-CUACE model was used to simulate a serious haze episode that occurred on 6–7 December 2013. The results demonstrate the model's suitability for describing haze episodes throughout China, especially in the Beijing–Tianjin–Hebei (Jing–Jin–Ji) region. A very close positive correlation was found between the southerly wind speed over the plain to the south of Beijing and changes in $PM_{2.5}$ in Beijing, both reaching maximum values at about 900 hPa, suggesting the lower atmosphere was the principal layer for pollutant PM transport from its southern neighboring region to Beijing. During haze episodes, and dependent upon the period, Beijing was either a pollution source or sink for its surrounding area. PM input from Beijing's environs was much higher than the output from the city, resulting in the most serious pollution episode, with the highest $PM_{2.5}$ values occurring from 0000 to 1000 UTC(0800 to 1800 LT) 7 December 2013. PM pollutants from the environs of the city accounted for over 50% of the maximum $PM_{2.5}$ values reached in Beijing. At other times, the Beijing area was a net contributor to pollution in its environs.

1. Introduction

Air pollution has become a serious problem in megacities around the world (*Kanakidou et al., 2011*), and the topic has been receiving increased attention because of the close relationship between air pollution and the atmospheric environment, human health and ecosystems (*Kan et al., 2012; Liu et al., 2012*). China's air pollution has become increasingly serious since the economic reforms of 1978, which allowed rapid economic development. Gross Domestic Product has grown by about 10% per annum (*China Statistical Yearbook 2012, 2013*). China is now considered as one of the engines of global economic growth, but this rapid growth has resulted in an increase in energy consumption, air pollution, and associated health effects (*Chan et al., 2008*).

In recent years, haze has become a major pollution problem in Chinese cities (*Wu et al., 2010; Du et al., 2011; Tan et al., 2011*). Under the observation standards released by the China Meteorological Administration (CMA), haze is defined as a pollution phenomenon characterized by deteriorated horizontal visibility of <10 km, caused by fine particulate matter (PM) suspended in the atmosphere (*CMA, 2003*). Haze occurs when sunlight is absorbed and scattered by high concentrations of atmospheric aerosols (*E. Kang et al., 2013; Salinas et al., 2013*). It has a negative impact on human health and the environment (*Wu et al., 2005; Gurjar et al., 2010*), and it also has climate change effect over a regional or global scale by altering solar and infrared radiation in the atmosphere (*Wang et al., 2011; Yu et al., 2011; Chen et al., 2012*).

With an increasing number of local and regional haze events reported by the media, much attention has been paid to reducing air pollutant emissions and to improving air quality across the cities (*Huang et al., 2013; H. Kang et*

al., 2013; Xu et al., 2013; Tan et al., 2014), municipalities, and provinces of China (*Cheng et al., 2014; Ji et al., 2014*). The Jing–Jin–Ji region, located in central-eastern China, is not only one of China's most economically developed and industrialized regions, but is the area that most frequently experiences haze episodes (*Ji et al., 2014; H. Wang, S.-C. Tan, et al., 2014; L. T. Wang et al., 2014*). Beijing, at the center of the Jing–Jin–Ji region, is one of China's most economically developed cities, and has suffered from increasingly severe haze events (*Duan et al., 2012; Wang et al., 2012; Liu et al., 2014; Quan et al., 2014*). It is vital that air pollution in Beijing is studied in detail so as to inform policy aimed at averting irreversible environmental damage (*Cheng et al., 2013; Zhang et al., 2014*). The other areas of the Jing–Jin–Ji region should also be studied, as they are important components of the wider region and affect Beijing directly via the transport of PM pollutants (*Fu et al., 2014; Ying et al., 2014*). In the present reported study, an online mesoscale haze forecasting model was used to study the transport of major air pollutants to and from Beijing and the other areas of the Jing–Jin–Ji region (*Wang et al., 2013*).

2. Modeling

2.1 Model description

The new-generation Global/Regional Assimilation and PrEdiction System (GRAPES_Meso) and the Chinese Unified Atmospheric Chemistry Environment (CUACE) model developed by the Chinese Academy of Meteorological Science (CAMS), the CMA, were integrated to build an online chemical weather forecasting model, GRAPES-CUACE, focusing especially on haze pollution forecasting in China and East Asia (*Zhang et al., 2008; Wang et al., 2009*). GRAPES_Meso was adopted as the numerical weather prediction model for aerosol determination. It is a new-generation general hydrostatic/non-hydrostatic, multi-scale numerical model developed by the

Research Center for Numerical Meteorological Prediction, CAMS, CMA (*Zhang and Shen, 2008*). The model uses standardized and module-based software and has been developed in accordance with strict software engineering requirements, including program-operated parallel calculations (*Xue et al., 2008*). Testing has shown that the design and application of the model meet these prerequisites, and that it can therefore serve as a good foundation for the sustainable development of a numerical prediction system for China (*Chen et al., 2008*). The large-scale horizontal and vertical transportation and diffusion processes for all gases and aerosols can also be processed using GRAPES_Meso's dynamic framework (*Xu et al., 2008*). Again, testing has demonstrated that both the design of the model's framework and its implementation meet the requirements of real-time operational weather forecasting, especially in China and East Asia. GRAPES_Meso has therefore been used as an operational, real-time, short-term weather prediction system in China since 2009 (*Yang et al., 2008; Zhu et al., 2008*).

The CUACE model was developed by the CAMS Centre for Atmosphere Watch And Services (CAWAS). It is a newly developed system for testing and forecasting air quality in China that includes four functions: treating aerosols; gas phase chemistry; emissions; and data assimilation (*Gong and Zhang, 2008*). The detailed data capture by this model of processes such as aerosol sources, transport, dry and wet deposition, and dust removal both in and below clouds, clearly describes the interaction between aerosols and clouds (*Zhou et al., 2008*). CUACE has been designed as a unified chemistry module that can be easily coupled with any atmospheric model (e.g. regional air quality and climate models) at various temporal and spatial scales. It has thus been integrated online with GRAPES_Meso to produce the GRAPES-CUACE model (*Wang et al., 2009,2010,2014c*). Dust particles are divided into 12 size bins(*Gong, 2003*), following guidelines provided by the measurement of soil

dust size in Chinese desert regions during 1994–2001(*Zhang, 2003*).

2.2 Model domain and parameters

In this study, GRAPES-CUACE was used to simulate a haze episode in December 2013. The model's vertical cap was set at about 30 km, with 31 vertical layers. As shown in Figure 1, its domain covered the East Asia region (20°–55°N, 90°–140°E) with a horizontal resolution of 0.25° × 0.25°. National Centers for Environmental Prediction (NCEP) 1° × 1° reanalysis data were used for the model's initial and six-hour meteorological lateral direction input fields. The model ran at 0000 UTC time everyday, based on NCEP reanalysis data and the chemical tracer initial field, and the simulation time is 48 hour. The monthly mean values of all tracers from observation data are used for initialization at the very beginning of the model run. The initial values of all gases in RADM2 and aerosol concentrations are based on the 24 h forecast made by the previous day's model run. The simulation results from 00 to 24 hours are used in this study. The model simulation begins from November 26 and the results of December 1-31 are used in order to avoid the uncertainties from the initial chemical fields at the model start.

3. Data description

This study employed CMA ground visibility and operational weather observation data. The data covered mainland China, including a total of 600 ground observation stations.

The daily mean $PM_{2.5}$ concentrations were from surface observations made by the China National Environmental Monitoring Center (CNEMC, http://www.cnpm25.com). They included values for 74 cities in mainland China. The data represented the mean values of data from different observation stations distributed in various downtown, suburb, and suburban areas of each city. For example, pollutant concentrations in Beijing were

obtained by extracting the mean value from the data from 12 observation sites. This value was then used to represent the mean pollution conditions for each city as a whole.

Detailed high-resolution emission inventories of reactive gases from emissions over China in 2007, i.e. for SO_2, NO_x, CO, NH_3, and volatile organic compounds (VOCs), were updated to form current emission data, based on official national emission source criteria *(Cao et al., 2006; 2010)*. The Sparse Matrix Operator Kernel Emissions (SMOKE) system was used to transform these emission data into the hourly-gridded data required by the GRAPES_CUACE model, including the five aerosol species of black carbon (BC), organic carbon (OC), sulfate, nitrate, and fugitive dust particles, in addition to 27 gases, such as VOCs, NH_3, CO, CO_2, SO_x and NO_X *(An et al., 2013)*. Modified SMOKE was used according to GRAPES_CUACE, which is similar to RADM II chemical mechanism. The detailed introduction of chemical species and chemical mechanism were given in the several papers (*Gong and Zhang, 2008; Wang et al., 2015*).

4. Results

4.1 Model evaluation

First, the simulation results were compared with the observation data from the major cities in the Jing–Jin–Ji region during the haze episode of 6–7 December to evaluate the model's capabilities. The Jing-Jin-Ji region and the Yangtze River Delta (YRD) region were the most severely polluted during 6–7 December, with mean observed $PM_{2.5}$ values for the two-day period of about 200 $\mu g/m^3$ (Fig. 1). The simulated PM2.5 concentrations are in good agreement with observations for most of the cities, especially in the Jing–Jin–Ji region (e.g. Baoding (BD), Beijing (BJ), Cangzhou (CZ), Chengde (CD), Dezhou (DZ), Jinan (JN), Handan (HD), Hengshui (HS), Qinhuangdao (QHD),

Shijiazhuang (SJZ), Tianjin (TJ), Xingtai (XT) and Zhangjiakou (ZJK)). Both datasets showed that cities in the northern Jing–Jin–Ji region experienced lower levels of pollution and were less affected by $PM_{2.5}$ during this haze episode (e.g. ZJK, CD, and QHD, with observed $PM_{2.5}$ concentrations of 59.1, 51.9 and 94.1 μg/m^3, respectively, and simulated $PM_{2.5}$ concentrations of 30.9, 44.3 and 60.1 μg/m^3, respectively), while the cities in the central and southern sectors of the Jing–Jin–Ji region experienced severe pollution and high $PM_{2.5}$ levels (e.g. BJ, TJ, BD, CZ, SJZ, HS, XT, HD, DZ and JN, with observed $PM_{2.5}$ concentrations of 194.3, 165.6, 302.1, 237.3, 268.7, 160.1, 295.1, 223.3, 224.3 and 149.9 μg/m^3, respectively, and simulated $PM_{2.5}$ concentrations of 115.7, 207.1, 250.1, 267.0, 237.7, 326.5, 323.3, 263.6, 312.1 and 256.1 μg/m^3, respectively). The modeled results thus accurately described the haze episode over the whole region.

The horizontal distribution of simulated $PM_{2.5}$ concentrations was compared with observed haze weather phenomena in eastern China. The centralized hazy weather observed in the region at 1400 UTC(2200 LT) 7 December 2013 corresponded with the area of high simulated $PM_{2.5}$ (Fig. 2). Simulated $PM_{2.5}$ values were >150 μg/m^3 for the whole of eastern China, with most areas of the highest concentration reaching 300 μg/m^3 or even 500 μg/m^3. Hazy weather was concentrated in the Jing–Jin–Ji region, i.e. Shandong, Jiangsu, and Zhejiang provinces, and Shanghai. There were clearly delineated areas of high simulated $PM_{2.5}$ values that corresponded with these regions.

There was an obvious demarcation line with respect to observed visibility from the southwest to the northeast, dividing China into high visibility and low visibility regions, with the low visibility region centered on the YRD (Fig. 3). The simulated visibility showed similar results (Fig. 3), albeit it was lower than the observed visibility in Shandong, southern Hebei and Shanxi provinces.

Several major cities, including BJ, BD, CZ, DZ, HD, HS, SJZ, XT and Zhengzhou (ZZ) in the Jing–Jin–Ji region and its environs, and Shanghai (SH) and Nanjing (NJ) in the YRD, were selected for a comparison of daily average observed and simulated $PM_{2.5}$ values during 1–31 December 2013, to test the validity of long-term simulations. As shown in Figure 4, the simulated daily results were fairly close to the observed values for the 6–7 December haze episode. Beginning on 6 December, this episode was most severe on 7 December; and then $PM_{2.5}$ levels decreased rapidly from 8 December onwards. The simulated results for Beijing and the average of whole Jing-Jin-Ji region were highly consistent with the trends in observed daily values for the whole of December. Simulated results for the other cities in the Jing–Jin–Ji region also showed close correlation with observed data for 6–7 December, even considering that the maximum value appeared one day earlier in HS and one day later in SH. While the simulated values for NJ were lower than the observed data, they essentially exhibited the same daily trends.

The results obtained by GRAPES-CUACE for the Jing–Jin–Ji region through its simulation of $PM_{2.5}$ concentrations demonstrate the model's suitability for studying the impact of particulate transport on $PM_{2.5}$ concentrations. The Jing–Jin–Ji region was therefore chosen as an appropriate study area.

4.2 Wind field

Beijing is currently experiencing the severest haze pollution in its history. On the plains of Hebei to the south, the most seriously polluted area in China, haze and fog episodes are much more serious even than in Beijing. Seven of the 10 cities with the highest levels of $PM_{2.5}$ pollution in China are located in this region (*Wang et al., 2014a, 2014b*). The contribution made by cross-city pollutants transported from southern Hebei Province to levels of $PM_{2.5}$ pollution in BJ is receiving much attention. The construction of the wind field

over this region, particularly the wind field pattern in the planetary boundary layer (PBL), is a key factor in determining the impact of the cross-city transport of $PM_{2.5}$ pollutants.

The wind field was analyzed to study the impact that PM transport from its environs had on air pollution in BJ during the haze episode of the present study. As Figure 5a shows, $PM_{2.5}$ concentrations in BJ reached their maximum at 0800 UTC(1600 LT) 7 December. Stable southwesterly winds affected BJ and the area to the south of BJ, while the wind direction was northwesterly and the wind speed lower in the region to the north of BJ. From both the observed and simulated data (Figs. 1, 2, and 3), it is apparent that the region to the south of BJ was the most polluted area, with the highest $PM_{2.5}$, lowest visibility and densest haze, and this region was therefore the likely main contributor to pollution levels in BJ during this haze episode. The vertical section along 115.25°E (Fig. 5b) enabled us to explore the relationship between the wind field and $PM_{2.5}$ concentrations and transport at different vertical heights. Figure 5b shows a southwesterly wind at 39°N blowing from the surface to the 800 hPa level in the region's southern sector. In the southern sector closest to BJ, the southerly wind speed reached its maximum value at about 900 hPa; and $PM_{2.5}$ also exhibited high values at the same height. Pollutants could thus be transported to BJ by the stable southwesterly wind from the southern environs via the 900 hPa layer. The northerly, or very weak southerly, wind in the region north of 41°N, together with the southerly wind south of 39°N, led to the formation of a wind convergence field over BJ stretching from the surface level to 900 hPa. This would have been beneficial to the accumulation of $PM_{2.5}$ and the consequent aggravation of haze. The vertical section along 39.375°N describes a southerly wind in the region to the south of BJ from 116°E to 125°E (Fig. 5c). This southerly wind, extending from the surface to 800 hPa, reached its maximum velocity at 900 hPa in the area to the south of BJ (116°E to 118°E). $PM_{2.5}$ concentrations were also

significantly higher in this region; pollutants from the 116°–125°E area would have been easily transported northward by the southerly wind. BJ was most likely affected by this process, raising pollution levels and aggravating the haze.

To verify these results, we analyzed the relationship between $PM_{2.5}$ concentrations in BJ and the wind field of the area to the south of BJ (i.e. 113.5°–118°E, 34.5°–39.5°N) (Fig. 5a). In the analysis, positive average hourly wind speed (*v*) values were representative of a southerly wind, and negative *v* values a northerly wind. The results showed that, when there was southerly wind in the area to the south of BJ, average $PM_{2.5}$ concentrations in BJ always increased (Fig. 6). This was most obvious on 7 December, when the highest $PM_{2.5}$ values occurred, accompanied by longer periods of stable southerly winds. When there was a northerly wind in the area to the south of BJ, average $PM_{2.5}$ concentrations in BJ fell, and then stabilized.

4.3 BJ's $PM_{2.5}$ input and output

To investigate the contribution of $PM_{2.5}$ transported from its surroundings to BJ pollution levels, the transport rates (kg/s) for $PM_{2.5}$ from four directions, east (E), west (W), south (S) and north (N), were calculated using the following formulas:

$$Tran_N(t) = \sum_{z=1}^{7} \sum_{x=x_1}^{x_2} PM_{y_1}(x,z,t) \cdot \Delta x_{y_1} \cdot \Delta z_{y_1}(x,z) \cdot v_{y_1}(x,z,t)$$

$$Tran_N(t) = \sum_{z=1}^{7} \sum_{x=x_1}^{x_2} PM_{y_1}(x,z,t) \cdot \Delta x_{y_1} \cdot \Delta z_{y_1}(x,z) \cdot v_{y_1}(x,z,t)$$

$$Tran_N(t) = \sum_{z=1}^{7} \sum_{x=x_1}^{x_2} PM_{y_1}(x,z,t) \cdot \Delta x_{y_1} \cdot \Delta z_{y_1}(x,z) \cdot v_{y_1}(x,z,t)$$

278 $$Tran_N(t) = \sum_{z=1}^{7} \sum_{x=x_1}^{x_2} PM_{y_1}(x,z,t) \cdot \Delta x_{y_1} \cdot \Delta z_{y_1}(x,z) \cdot v_{y_1}(x,z,t)$$

279 $$Tran_N(t) = \sum_{z=1}^{7} \sum_{x=x_1}^{x_2} PM_{y_1}(x,z,t) \cdot \Delta x_{y_1} \cdot \Delta z_{y_1}(x,z) \cdot v_{y_1}(x,z,t)$$

280 where $Tran_N$, $Tran_S$, $Tran_E$ and $Tran_W$ represent the $PM_{2.5}$ transport rate for N,
281 S, E and W, respectively (Fig. 7). Positive *Tran* values indicated net pollutant
282 input into BJ; negative *Tran* values described net pollutant output from BJ. PM
283 stands for $PM_{2.5}$ concentration; x_1, x_2 (Fig. 7) are the westernmost and
284 easternmost BJ longitudes, respectively, and the subscripts y_1, y_2 (Fig. 7) are
285 the southernmost and northernmost BJ latitudes; *t* stands for time; Δ*x*, Δ*y*, Δ*z*
286 indicate the individual grid distances of the *x*, *y*, *z* axes; *u* stands for the
287 easterly/westerly wind speed (negative for easterly wind); and *v* stands for the
288 southerly/northerly wind speed (negative for northerly wind). The constantly
289 negative $PM_{2.5}$ transport rate toward BJ, reaching a maximum rate of −112.8
290 kg/s at 1100 UTC(1900 LT) in the southerly direction, indicated a constant
291 output of $PM_{2.5}$ southward from BJ to its southern environs on 6 December
292 (Fig. 8a). Eastward $PM_{2.5}$ transport rates were largely negative before 1200
293 UTC(2000 LT), indicating net $PM_{2.5}$ output from BJ downwind. After 1200
294 UTC(2000 LT), the $PM_{2.5}$ transport rate became slightly positive and then
295 remained steady, indicating a small net input in the afternoon. There was little
296 westerly or northerly transport throughout the day.

297 The total input/output rate was calculated by summing the input/output
298 transport rate for the four directions; and the net transport rate was obtained
299 by summing the total input and output rate. Positive net transport values
300 indicated that the BJ area was receiving $PM_{2.5}$ from its surroundings; negative
301 net values showed BJ to be exporting $PM_{2.5}$ to its surroundings. The total
302 output rate clearly exceeded the input rate, and the net transport rate was
303 negative, indicating a net output of pollutants from BJ during the period 0000–

1300 UTC(0800-2100 LT) 6 December (Fig. 8b). After 1400 UTC(2200 LT), the output rate clearly fell, while the input rate remained substantially unchanged, resulting in the net transport rate falling close to zero. This shows that the BJ area was a source of pollutants for the areas to its east and south throughout the whole of 6 December.

For 7 December (the most polluted day in this episode), transport rate values for each direction changed substantially (Fig. 8c). There were large positive values for westerly and southerly winds, indicating major $PM_{2.5}$ transport from these directions to BJ; and this correlates with the inferences drawn from Figure 5 and Figure 6. The transport rate eastward was always positive, reaching a maximum of 149.5 kg/s at 0800 UTC(1600 LT); it was always negative in the westward direction, reaching a minimum of −174.2 kg/s at 1200 UTC(2000 LT). This suggests that a westerly wind dominated on 7 December and transported $PM_{2.5}$ from the area to the west of BJ to the city and to its eastern downwind area. $PM_{2.5}$ transport was heaviest at 0800 UTC(1600 LT) and 1200 UTC(2000 LT) from the west and east, respectively. There was input from the south and output northward before 1100 UTC(1900 LT), with concurrent maxima of 86.4 and 22.6 kg/s at 0800 UTC(1600 LT), respectively. After 1200 UTC(2000 LT), the wind direction became northerly, leading to a reversal in the direction of input/output pollutant transport. Net pollutant output turned southward; the output rate was clearly greater than the input rate from the north during the period 1200–2400 UTC 7 December(2000 LT 7 December to 0800 LT 8 December).

The net transport rate for BJ on 7 December was positive before 1000 UTC(1800 LT), rising from about zero to a maximum of 118.1 kg/s at 0600 UTC(1400 LT), and then began to decline to consistently negative values after 1100 UTC(1900 LT) (Fig. 8d). This suggests that the input of pollutants into BJ exceeded the output during the period 0000–1000 UTC(0800-1800 LT).

After 1100 UTC(1900 LT), input transport rates into BJ were markedly reduced, resulting in a net negative transport of pollutants, indicating that BJ was a source of pollutants for its environs. Combined with the results from Figure 8c, there was net pollutant output to BJ's east and south. By analyzing Figure 8c and Figure 8d, it can be seen that changes in the net transport rate for BJ correlated with the transport rate southward. This was principally because westerly input and easterly output were basically equal and so offset one another. The northward transport rate was consistently low, and the variable southward transport rate therefore had an enormous influence on the BJ area. These results indicate that pollutant transport between BJ and its southern environs had the most significant impact on pollution levels in BJ in comparison to other areas.

4.4 Contribution of pollutant transport to $PM_{2.5}$ concentrations over BJ

The observation studies of haze events in east China (Wang et al., 2014a) showed "there is an aerosol extinction layer from the height of 1-1.5 km to 2-3 km from the ground, indicating most of the PM10 pollutants are mainly concentrated in the near ground atmosphere layer below 1 km and a small part of pollutants can also spread to the height of more than 2-3 km from the ground". In order to evaluate the contribution made by pollutants transported from its environs to BJ $PM_{2.5}$ pollution, the total $PM_{2.5}$ suspended in the atmosphere between the surface and a height of 3000 m over the BJ area during this haze episode was calculated, according to the formula

$$Tran_N(t) = \sum_{z=1}^{7} \sum_{x=x_1}^{x_2} PM_{y_1}(x,z,t) \cdot \Delta x_{y_1} \cdot \Delta z_{y_1}(x,z) \cdot v_{y_1}(x,z,t),$$

along with the net hourly transport amount (Fig. 9). Total $PM_{2.5}$ changed little during 6 December, but did rise slightly after a small decline at 1200

UTC(2000 LT) when the net hourly output transport value decreased. The total $PM_{2.5}$ amount continued rising on 7 December and began to accelerate sharply until 0900 UTC(1700 LT) (4555.4 t) with a large net hourly input. After 1200 UTC(2000 LT), net hourly transport became highly negative, and total $PM_{2.5}$ decreased rapidly. By the end of 7 December, the total $PM_{2.5}$ suspended in the atmosphere over BJ was consistent with the values for 6 December. As Figure 9 shows, this sharp rise in total $PM_{2.5}$ began at 1200 UTC(2000 LT) on 6 December(980t), and ended at 1200 UTC(2000 LT) on 7 December(3707t), when total $PM_{2.5}$ reached its maximum value before beginning to decrease, and the total $PM_{2.5}$ suspended over the BJ area increased by about 2727 t in this period. As the calculation results in Table 1 show, net input was 1497 t, accounting for 55% of the total $PM_{2.5}$ increase(2727t) from 1200 UTC(2000 LT) 6 December to 1200 UTC(2000 LT) 7 December. The remaining 1230 t could be attributed to local effects, and accounted for 45% of the total $PM_{2.5}$ increase (Fig. 10). This suggests that the transport of particle pollutants from its environs made a significant contribution to the peak $PM_{2.5}$ values over BJ during this haze episode.

5. Conclusion

The GRAPES-CUACE online mesoscale chemical weather forecasting model was used to study the influence of PM transported from its near environs on high $PM_{2.5}$ pollution levels in BJ during a severe haze episode on 6–7 December 2013. Simulated results were compared with ground-level horizontal visibility, haze weather phenomena as observed by CMA, and surface $PM_{2.5}$ concentrations observed by CNEMC, to evaluate the model's ability to accurately describe haze pollution in China. The 3D wind field over the Jing–Jin–Ji region and its relationship with $PM_{2.5}$ variations in BJ, the input/output pollutant transport rates for BJ and its N, S, E and W environs, the total input, output and net pollutant transport amounts for BJ, and the total

386 $PM_{2.5}$ suspended in the atmosphere over BJ, were all calculated in relation to
387 the possible contribution of $PM_{2.5}$ transported from its environs to the high
388 $PM_{2.5}$ pollution levels in BJ during the aforementioned severe haze episode.
389 The results can be summarized as follows:

390 (1) The spatial and temporal comparison of the simulated results with
391 observational data showed that the model is capable of accurately describing
392 haze episodes in China, and especially in the Jing–Jin–Ji region. This then
393 formed a sound foundation for the calculation of PM transported across cities
394 in this region.

395 (2) There was a very close positive correlation between the southerly
396 wind speed over the area to the south of BJ and $PM_{2.5}$ variations in BJ,
397 suggesting the likely important contribution made by PM transport from BJ's
398 southern environs to the city. At 0800 UTC(1600 LT) on 7 December,
399 southwesterlies from the surface to 800 hPa were largely stable in BJ and its
400 southern environs; the region north of BJ was affected by a gentle wind. Both
401 the southerly wind speed in the area to the south of BJ, and $PM_{2.5}$, reached
402 their maxima at about 900 hPa, suggesting this height served as the major
403 transport layer for pollutants from the south to BJ.

404 (3) The BJ area was a net output source for its environs for most of the
405 haze episode during 6–7 December, except for the period from 0000 to 1000
406 UTC(0800 to 1800 LT) 7 December, when the haze was at its most serious
407 and was accompanied by the highest $PM_{2.5}$ values. Input from the west was
408 more or less offset by transport eastward. The input rate from the south was
409 much higher than the output rate to the north from 0000 to 1000 UTC(0800 to
410 1800 LT) 7 December, and there was thus a net input during this period,
411 resulting in the most serious pollution levels and peak $PM_{2.5}$ values for this
412 haze episode. This shows that pollutant transport from the south was the
413 major contributor to the peak $PM_{2.5}$ pollution levels in the BJ area.

(4) Total $PM_{2.5}$ suspended in the atmosphere from the surface to 3000 m over the BJ area changed very little during 6 December. Total $PM_{2.5}$ began to rise slightly at 1200 UTC(2000 LT) 6 December, when the net hourly output transport rate decreased; then rose clearly at 0000 UTC(0800 LT) 7 December; and was followed by a rising trend that maintained until 0900 UTC(1700 LT) 7 December, accompanied by high net hourly input values. After 1200 UTC(2000 LT), the net hourly transport rate became significantly negative as total $PM_{2.5}$ decreased rapidly. Total $PM_{2.5}$ suspended over BJ increased by about 2727 t from 1200 UTC(2000 LT) 6 December to 1200 UTC(2000 LT) 7 December. The total net input was 1497 t, accounting for 55% of the total $PM_{2.5}$ increase during this period. The remaining 1230 t could be attributed to local effects, and accounted for 45% of the total $PM_{2.5}$ increase. This suggests that PM transport from its environs significantly influenced the peak $PM_{2.5}$ values over BJ during this episode.

Acknowledgements

This work was supported by the National Basic Research Program (973) (Grant No. 2014CB441201), the National Natural Scientific Foundation of China (Grant Nos. 41275007 & 41130104), the Jiangsu Collaborative Innovation Center for Climate Change， CAMS key projects (Grant No. 2013Z007), the Science and Technology Support Program of Jiangsu Province (Grant No. BE2012771), and the Priority Academic Program Development of Jiangsu Higher Education Institutions (PAPD).

437 **References**

438 An, X. Q., Sun, Z. B., Lin, W. l., Jin, M., and Li, N.: Emission inventory
439 evaluation using observations of regional atmospheric background
440 stations of China, J. Environ. Sci., 25, 537–546, 2013.
441 Cao, G., Zhang, X., and Zheng, F.: Inventory of black carbon and organic
442 carbon 446 emissions from China, Atmos. Environ., 40, 6516–27, 2006.
443 Cao, G. L., AN, X. Q., Zhou, C. H., Ren, Y. Q., and Tu, J.: Emission inventory
444 of air pollutants in China, Chin. Environ. Sci., 30, 900–906, 2010.
445 Chan, C. K. and Yao, X.: Air pollution in mega cities in China, Atmos. Environ.,
446 42, 1–42, doi:10.1016/j.atmosenv.2007.09.003, 2008.**TS3**
447 Chen, D., Xue, J., Yang, X., Zhang, H., Shen, X., Hu, J., Wang, Y., Ji, L., and
448 Chen, J.: New generation of multi-scale NWP system (GRAPES): general
449 scientific design, Chinese Sci. Bull., 53, 3433–3445, doi:10.1007/s11434-
450 008-0494-z, 2008.
451 Chen, Y., Liu, Q., Geng, F., Zhang, H., Cai, C., Xu, T., Ma, X., and Li, H.:
452 Vertical distribution of optical and micro-physical properties of ambient
453 aerosols during dry haze periods in Shanghai, Atmos. Environ., 50, 50–
454 59, doi:10.1016/j.atmosenv.2012.01.002, 2012.
455 Cheng, Y., Engling, G., He, K.-B., Duan, F.-K., Ma, Y.-L., Du, Z.-Y., Liu, J.-M.,
456 Zheng, M., and Weber, R. J.: Biomass burning contribution to Beijing
457 aerosol, Atmos. Chem. Phys., 13, 7765–7781, doi:10.5194/acp-13-7765-
458 2013, 2013.
459 Cheng, Z., Wang, S., Fu, X., Watson, J. G., Jiang, J., Fu, Q., Chen, C., Xu, B.,
460 Yu, J., Chow, J. C., and Hao, J.: Impact of biomass burning on haze
461 pollution in the Yangtze River delta, China: a case study in summer 2011,
462 Atmos. Chem. Phys., 14, 4573–4585, doi:10.5194/acp-14- 4573-2014,
463 2014.
464 China Statistical Yearbook 2012, 2013, National Bureau of Statistics of China,
465 China Statistics Press, Beijing, 2012, 2013.
466 CMA: Specifications for the Surface Meteorological Observations, Meteoro-

467 logical Press, Beijing, China (in Chinese), 2003.
468 Du, H., Kong, L., Cheng, T., Chen, J., Du, J., Li, L., Xia, X., Leng, C., and
469 Huang, G.: Insights into summertime haze pollution events over Shanghai
470 based on online water-soluble ionic com- position of aerosols, Atmos.
471 Environ., 45, 5131–5137, doi:10.1016/j.atmosenv.2011.06.027, 2011.
472 Duan, J., Guo, S., Tan, J., Wang, S., and Chai, F.: Characteristics of
473 atmospheric carbonyls during haze days in Beijing, China, Atmos. Res.,
474 114–115, 17–27, doi: 10.1016/j.atmosres.2012.05.010, 2012.
475 Fu, X., Wang, S. X., Cheng, Z., Xing, J., Zhao, B., Wang, J. D., and Hao, J.
476 M.: Source, transport and impacts of a heavy dust event in the Yangtze
477 River Delta, China, in 2011, Atmos. Chem. Phys., 14, 1239–1254,
478 doi:10.5194/acp-14-1239-2014, 2014.
479 Gong, S. L.: Characterization of soil dust aerosol in China and its transport
480 and distribution during 2001 ACE-Asia: 2. Model simulation and validation,
481 J. Geophys. Res., 108, doi:10.1029/2002jd002633, 2003.
482 Gong, S. L. and Zhang, X. Y.: CUACE/Dust – an integrated system of
483 observation and modeling systems for operational dust forecasting in
484 Asia, Atmos. Chem. Phys., 8, 2333–2340, doi:10.5194/acp-8-2333-2008,
485 2008.
486 Gurjar, B. R., Jain, A., Sharma, A., Agarwal, A., Gupta, P., Nagpure, A. S., and
487 Lelieveld, J.: Human health risks in megacities due to air pollution, Atmos.
488 Environ., 44, 4606–4613, doi:10.1016/j.atmosenv.2010.08.011, 2010.
489 Huang, K., Zhuang, G., Lin, Y., Wang, Q., Fu, J. S., Fu, Q., Liu, T., and Deng,
490 C.: How to improve the air quality over megacities in China: pollution
491 characterization and source analysis in Shanghai before, during, and after
492 the 2010 World Expo, Atmos. Chem. Phys., 13, 5927– 5942,
493 doi:10.5194/acp-13-5927-2013, 2013.
494 Ji, D., Li, L., Wang, Y., Zhang, J., Cheng, M., Sun, Y., Liu, Z., Wang, L., Tang,
495 G., Hu, B., Chao, N., Wen, T., and Miao, H.: The heaviest particulate air-
496 pollution episodes occurred in northern China in January, 2013: insights

497 gained from observation, Atmos. Environ., 92, 546–556,
498 doi:10.1016/j.atmosenv.2014.04.048, 2014.
499 Kan, H., Chen, R., and Tong, S.: Ambient air pollution, climate change, and
500 population health in China, Environ Int., 42, 10–19,
501 doi:10.1016/j.envint.2011.03.003, 2012.
502 Kanakidou, M., Mihalopoulos, N., Kindap, T., Im, U., Vrekoussis, M.,
503 Gerasopoulos, E., Der- mitzaki, E., Unal, A., Koçak, M., Markakis, K.,
504 Melas, D., Kouvarakis, G., Youssef, A. F., Richter, A., Hatzianastassiou,
505 N., Hilboll, A., Ebojie, F., Wittrock, F., von Savigny, C., Burrows, J. P.,
506 Ladstaetter-Weissenmayer, A., and Moubasher, H.: Megacities as hot
507 spots of air pollution in the East Mediterranean, Atmos. Environ., 45,
508 1223–1235, doi: 10.1016/j.atmosenv.2010.11.048, 2011.
509 Kang, E., Han, J., Lee, M., Lee, G., and Kim, J. C.: Chemical characteristics
510 of size-resolved aerosols from Asian dust and haze episode in Seoul
511 Metropolitan City, Atmos. Res., 127, 34–46,
512 doi:10.1016/j.atmosres.2013.02.002, 2013.
513 Kang, H., Zhu, B., Su, J., Wang, H., Zhang, Q., and Wang, F.: Analysis of a
514 long-lasting haze episode in Nanjing, China, Atmos. Res., 120–121, 78–
515 87, doi: 10.1016/j.atmosres.2012.08.004, 2013.
516 Liu, Q., Liu, Y., Yin, J., Zhang, M., and Zhang, T.: Chemical characteristics and
517 source apportionment of PM10 during Asian dust storm and non-dust
518 storm days in Beijing, Atmos. Environ., 91, 85–94,
519 doi:10.1016/j.atmosenv.2014.03.057, 2014.
520 Liu, W.-T., Hsieh, H.-C., Chen, S.-P., Chang, J. S., Lin, N.-H., Chang, C.-C.,
521 and Wang, J.-L.: Diagnosis of air quality through observation and
522 modeling of volatile organic compounds (VOCs) as pollution tracers,
523 Atmos. Environ., 55, 56–63, doi:10.1016/j.atmosenv.2012.03.017, 2012.
524 Quan, J., Tie, X., Zhang, Q., Liu, Q., Li, X., Gao, Y., and Zhao, D.:
525 Characteristics of heavy aerosol pollution during the 2012–2013 winter in
526 Beijing, China, Atmos. Environ., 88, 83–89,

527 doi:10.1016/j.atmosenv.2014.01.058, 2014.
528 Salinas, S. V., Chew, B. N., Miettinen, J., Campbell, J. R., Welton, E. J., Reid,
529 J. S., Yu, L. E., and Liew, S. C.: Physical and optical characteristics of the
530 October 2010 haze event over Singapore: a photometric and lidar
531 analysis, Atmos. Res., 122, 555–570,
532 doi:10.1016/j.atmosres.2012.05.021, 2013.
533 Tan, J., Guo, S., Ma, Y., Duan, J., Cheng, Y., He, K., and Yang, F.:
534 Characteristics of particulate PAHs during a typical haze episode in
535 Guangzhou, China, Atmos. Res., 102, 91–98,
536 doi:10.1016/j.atmosres.2011.06.012, 2011.
537 Tan, J., Yang, L., Grimmond, C. S. B., Shi, J., Gu, W., Chang, Y., Hu, P., Sun,
538 J., Ao, X., and Han, Z.: Urban integrated meteorological observations:
539 practice and experience in Shanghai, China, B. Am. Meteorol. Soc.,
540 140602092802009, doi:10.1175/bams-d-13-00216.1, 2014.
541 Wang, G., Chen, C., Li, J., Zhou, B., Xie, M., Hu, S., Kawamura, K., and
542 Chen, Y.: Molecular composition and size distribution of sugars, sugar-
543 alcohols and carboxylic acids in airborne particles during a severe urban
544 haze event caused by wheat straw burning, Atmos. Environ., 45, 2473–
545 2479, doi:10.1016/j.atmosenv.2011.02.045, 2011.
546 Wang, H., Gong, S., Zhang, H., Chen, Y., Shen, X., Chen, D., Xue, J., Shen,
547 Y., Wu, X., and Jin, Z.: A new-generation sand and dust storm forecasting
548 system GRAPES_CUACE/Dust: model development, verification and
549 numerical simulation, Chinese Sci. Bull., 55, 635–649,
550 doi:10.1007/s11434-009-0481-z, 2009.
551 Wang, H., Zhang, X., Gong, S., Chen, Y., Shi, G., and Li, W.: Radiative
552 feedback of dust aerosols on the East Asian dust storms, J. Geophys.
553 Res., 115, doi:10.1029/2009jd013430, 2010.
554 Wang, H., Shi, G., Zhu, J., Chen, B., Che, H., and Zhao, T.: Case study of
555 longwave contribution to dust radiative effects over East Asia, Chinese
556 Sci. Bull., 58, 3673–3681, doi:10.1007/s11434-013-5752-z, 2013.

Wang, H., Tan, S.-C., Wang, Y., Jiang, C., Shi, G.-y., Zhang, M.-X., and Che, H.-Z.: A multisource observation study of the severe prolonged regional haze episode over eastern China in January 2013, Atmos. Environ., 89, 807–815, doi:10.1016/j.atmosenv.2014.03.004, 2014a.

Wang, H., Xu, J., Zhang, M., Yang, Y., Shen, X., Wang, Y., Chen, D., and Guo, J.: A study of the meteorological causes of a prolonged and severe haze episode in January 2013 over central-eastern China, Atmos. Environ., 98, 146–157, doi:10.1016/j.atmosenv.2014.08.053, 2014b.

Wang, H., Shi, G. Y., Zhang, X. Y., Gong, S. L., Tan, S. C., Chen, B., Che, H. Z., and Li, T.: Mesoscale modeling study of the interactions between aerosols and PBL meteorology during a haze episode in China Jing-Jin-Ji and its near surrounding region – Part 2: Aerosols' radiative feedback effects. Atmospheric Chemistry and Physics Discussions, 14(20), 28269-28298, doi: 10.5194/acpd-14-28269-2014,2014c.

Wang, H., Xue, M., Zhang, X. Y., Liu, H. L., Zhou, C. H., Tan, S. C., Che, H. Z., Chen, B., and Li, T.: Mesoscale modeling study of the interactions between aerosols and PBL meteorology during a haze episode in Jing–Jin–Ji (China) and its nearby surrounding region – Part 1: Aerosol distributions and meteorological features. Atmospheric Chemistry and Physics*, 15*(6), 3257-3275, doi: 10.5194/acp-15-3257-2015, 2015.

Wang, L., Xu, J., Yang, J., Zhao, X., Wei, W., Cheng, D., Pan, X., and Su, J.: Understanding haze pollution over the southern Hebei area of China using the CMAQ model, Atmos. Environ., 56, 69–79, doi:10.1016/j.atmosenv.2012.04.013, 2012.

Wang, L. T., Wei, Z., Yang, J., Zhang, Y., Zhang, F. F., Su, J., Meng, C. C., and Zhang, Q.: The 2013 severe haze over southern Hebei, China: model evaluation, source apportionment, and policy implications, Atmos. Chem. Phys., 14, 3151–3173, doi:10.5194/acp-14-3151-2014, 2014.

Wu, D., Tie, X., Li, C., Ying, Z., Kai-Hon Lau, A., Huang, J., Deng, X., and Bi, X.: An extremely low visibility event over the Guangzhou region: a case

study, Atmos. Environ., 39, 6568– 6577, doi:10.1016/j.atmosenv.2005.07.061, 2005.

Wu, D., Wu, X. J., Li, F., Tan, J., Chen, Z. Q., Cao, X., Sun, H. H., Chen, and Li, H. Y.: Temporal and spatial variation of haze during 1951–2005 in Chinese mainland, Meteorologica Sinica, 68, 680–688, 2010.

Xu, G., Chen, D., Xue, J., Sun, J., Shen, X., Shen, Y., Huang, L., Wu, X., Zhang, H., and Wang, S.: The program structure designing and optimizing tests of GRAPES physics, Chi- nese Sci. Bull., 53, 3470–3476, doi:10.1007/s11434-008-0418-y, 2008.

Xu, H. M., Tao, J., Ho, S. S. H., Ho, K. F., Cao, J. J., Li, N., Chow, J. C., Wang, G. H., Han, Y. M., Zhang, R. J., Watson, J. G., and Zhang, J. Q.: Characteristics of fine particulate non-polar organic compounds in Guangzhou during the 16th Asian Games: effectiveness of air pollution controls, Atmos. Environ., 76, 94–101, doi: 10.1016/j.atmosenv.2012.12.037, 2013.

Xue, J., Zhuang, S., Zhu, G., Zhang, H., Liu, Z., Liu, Y., and Zhuang, Z.: Scientific design and preliminary results of three-dimensional variational data assimilation system of GRAPES, Chinese Sci. Bull., 53, 3446–3457, doi:10.1007/s11434-008-0416-0, 2008.

Yang, X., Hu, J., Chen, D., Zhang, H., Shen, X., Chen, J., and Ji, L.: Verification of GRAPES unified global and regional numerical weather prediction model dynamic core, Chinese Sci. Bull., 53, 3458–3464, doi: 10.1007/s11434-008-0417-z, 2008.

Ying, Q., Wu, L., and Zhang, H.: Local and inter-regional contributions to PM2.5 nitrate and sulfate in China, Atmos. Environ., doi:10.1016/j.atmosenv.2014.05.078, 2014.

Yu, X., Zhu, B., Yin, Y., Yang, J., Li, Y., and Bu, X.: A comparative analysis of aerosol properties in dust and haze-fog days in a Chinese urban region, Atmos. Res., 99, 241–247, doi:10.1016/j.atmosres.2010.10.015, 2011.

Zhang, R. and Shen, X.: On the development of the GRAPES – a new

generation of the national operational NWP system in China, Chinese Sci. Bull., 53, 3429–3432, doi: 10.1007/s11434- 008-0462-7, 2008.

Zhang, S., Wu, Y., Wu, X., Li, M., Ge, Y., Liang, B., Xu, Y., Zhou, Y., Liu, H., Fu, L., and Hao, J.: Historic and future trends of vehicle emissions in Beijing, 1998–2020: A policy assessment for the most stringent vehicle emission control program in China, Atmos. Environ., 89, 216–229, doi:10.1016/j.atmosenv.2013.12.002, 2014.Zhang, X. Y.: Sources of Asian dust and role of climate change versus desertification in Asian dust emission, Geophys. Res. Lett., 30, doi:10.1029/2003gl018206, 2003.

Zhou, C. H., Gong, S. L., Zhang, X. Y., Wang, Y. Q., Niu, T., Liu, H. L., Zhao, T. L., Yang, Y. Q., and Hou, Q.: Development and evaluation of an operational SDS forecasting system for East Asia: CUACE/Dust, Atmos. Chem. Phys., 8, 787–798, doi:10.5194/acp-8-787-2008, 2008.

Zhu, G., Xue, J., Zhang, H., Liu, Z., Zhuang, S., Huang, L., and Dong, P.: Direct assimilation of satellite radiance data in GRAPES variational assimilation system, Chinese Sci. Bull., 53, 3465–3469, doi:10.1007/s11434-008-0419-x, 2008.

635 Figure captions

636 Fig. 1 Mean observed and simulated PM2.5 (μg/m3) for 6–7 December 2013

637 Fig. 2 Simulated PM2.5 (shaded) and haze weather phenomena observed at
638 1400 UTC(2200 LT) 7 December 2013

639 Fig. 3 Mean (a) observed and (b) simulated visibility for 6–7 December 2013

640 Fig. 4 Daily variations in observed and simulated PM2.5 (μg/m3) for 1–31
641 December 2013 at stations in BJ, BD, CZ, DZ, HD, HS, NJ, SH, SJZ, XT, ZZ
642 and the whole Jing-jin-ji

643 Fig. 5 (a) Horizontal wind field at 900 hPa, its vertical section at (b) 115.25°E
644 and (c) 39.375°N at 0800 UTC(1600 LT) 7 December 2013

645 Fig. 6 Hourly variations in PM2.5 (μg/m3) in BJ and mean southerly wind
646 speed (negative for northerly wind) for the region to the south of BJ, 1–10
647 December 2013

648 Fig. 7 Schematic diagram of pollutant transport between BJ and its
649 surrounding regions

650 Fig. 8 PM2.5 transport rates (kg/s) from S, N, W and E of BJ on (a) 6 and (c) 7
651 December. Total input, output and net PM2.5 transport rate (kg/s) from BJ's
652 environs on (b) 6 and (d) 7 December

653 Fig. 9 Total PM2.5 (ton) suspended in the atmosphere from the surface to
654 3000 m over the BJ area and the net hourly PM2.5 input (ton/h) for BJ during
655 6–7 December 2013

656 Fig. 10 Contribution made by net transport and local effects to PM2.5
657 increases in BJ, 6–7 December 2013
658

659

660 Table 1 Total input, total output and total net transport (all in tons) for the BJ
661 area for each time period (UTC and LT) during 6–7 December 2013

Time(UTC)	Time(LT)	Input	Output	Net
0000–1200 6 Dec	0800 6 Dec-2000 6 Dec	2032	−4854	−2822
1200–2400 6 Dec	2000 6 Dec-0800 7 Dec	1850	−2617	−767
0000–1200 7 Dec	0800 7 Dec-2000 7 Dec	6551	−4288	2264
1200–2400 7 Dec	2000 7 Dec-0800 8 Dec	3523	−6653	−3130
0000–2400 6 Dec	0800 6 Dec-0800 7 Dec	3882	−7471	−3588
0000–2400 7 Dec	0800 7 Dec-0800 8 Dec	10074	−10940	−866
0000 6 Dec–2400 7 Dec	0800 6 Dec-0800 8 Dec	13956	−18411	−4455
1200 6 Dec–1200 7 Dec	2000 6 Dec-2000 7 Dec	8401	−6905	1497

662
663
664 Table 2 Station locations

Station	Lat.	Long.	Alt. (m)
Beijing (BJ)	39.90	116.47	31.3
Shijiazhuang (SJZ)	38.05	114.43	80.5
Baoding (BD)	38.51	115.30	17.2
Cangzhou (CZ)	38.18	116.52	9.6
Dezhou (DZ)	37.26	116.17	21.2
Handan (HD)	36.36	114.28	58.2
Hengshui (HS)	37.44	115.42	24.3
Xingtai (XT)	37.04	114.30	76.8
Zhengzhou (ZZ)	34.73	113.70	110.4
Nanjing (NJ)	32.05	118.77	8.9
Shanghai (SH)	31.23	121.48	4.5

665
666

667 Fig. 1 Mean observed and simulated $PM_{2.5}$ (μg/m3) for 6–7 December 2013

668

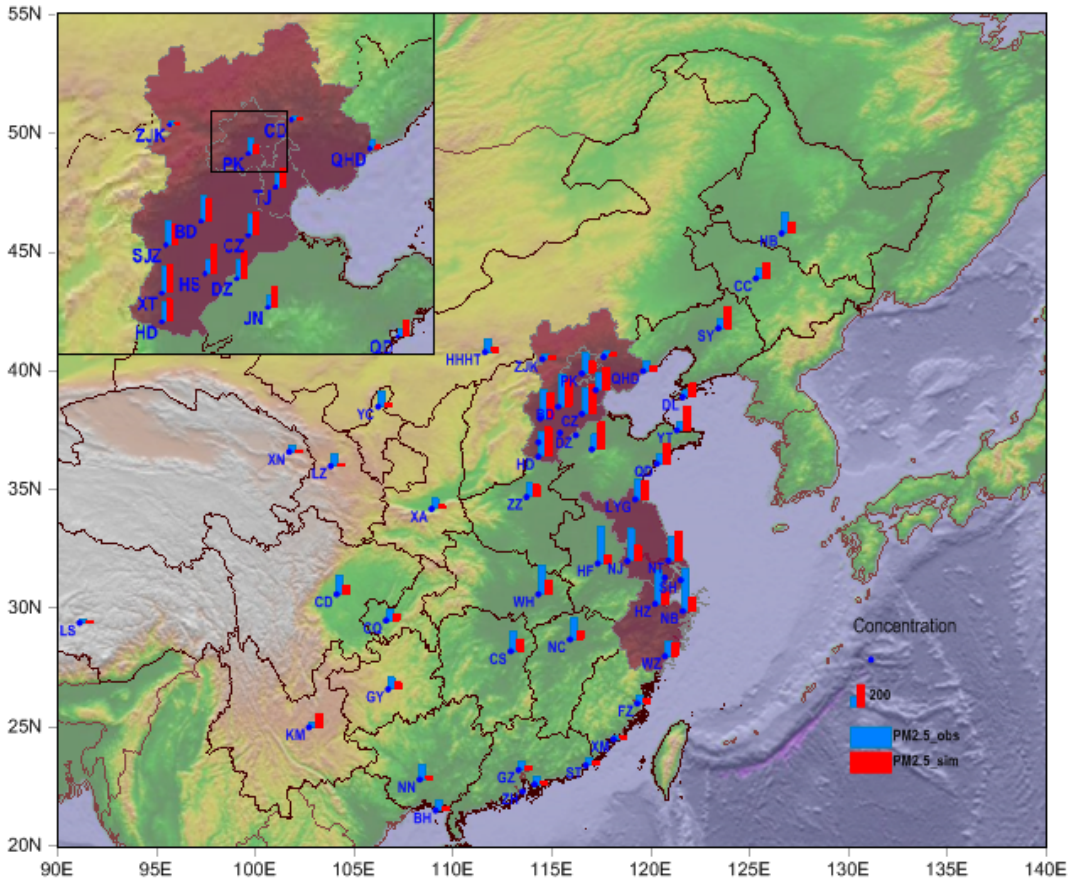

669

670

671 Fig. 2 Simulated $PM_{2.5}$ (shaded) and haze weather phenomena observed at
672 1400 UTC(2200 LT) 7 December 2013

673

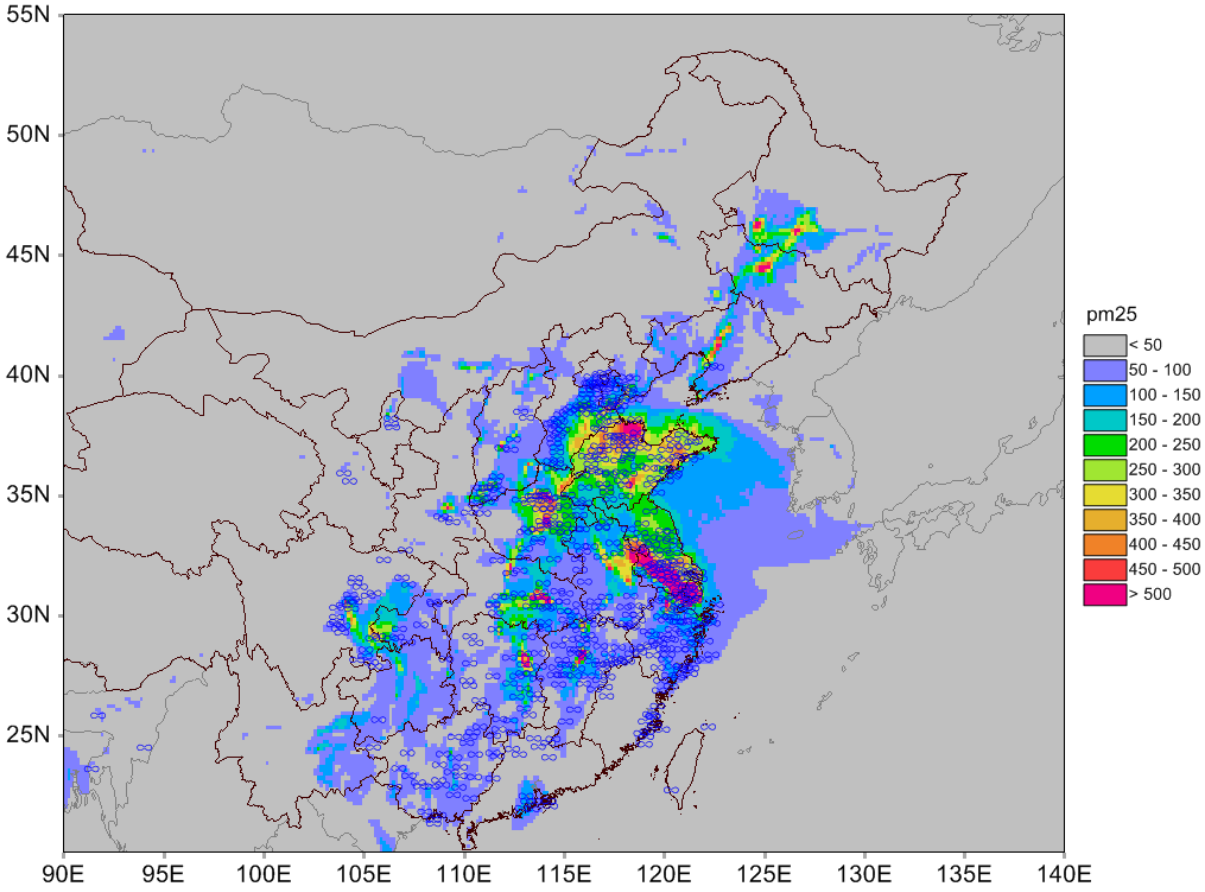

674

675 Fig. 3 Mean observed and simulated visibility for 6–7 December 2013

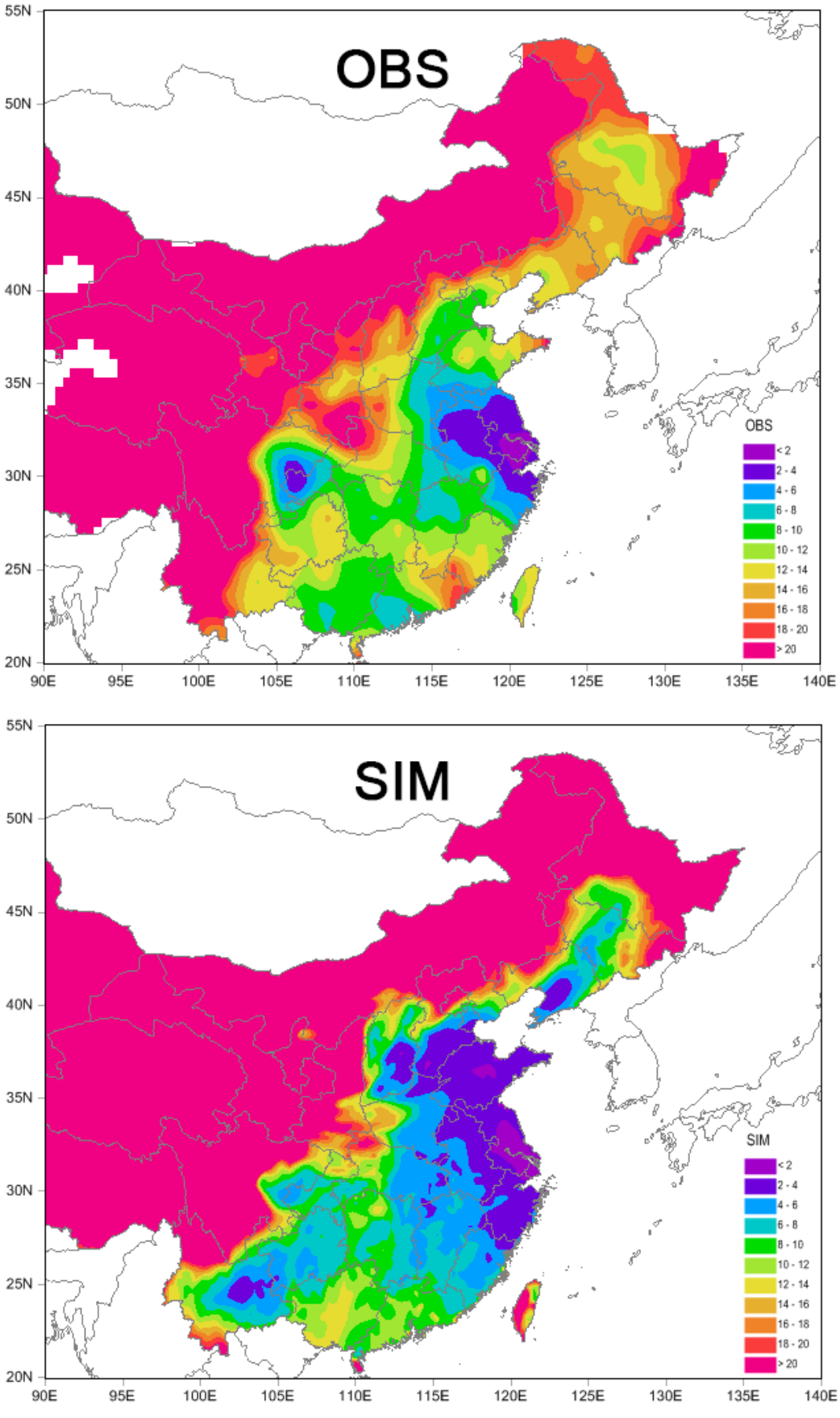

676

677 Fig. 4 Daily variations in observed and simulated $PM_{2.5}$ (μg/m3) for 1–31
678 December 2013 at stations in BJ, BD, CZ, DZ, HD, HS, NJ, SH, SJZ, XT, ZZ
679 and the whole Jing-jin-ji.
680

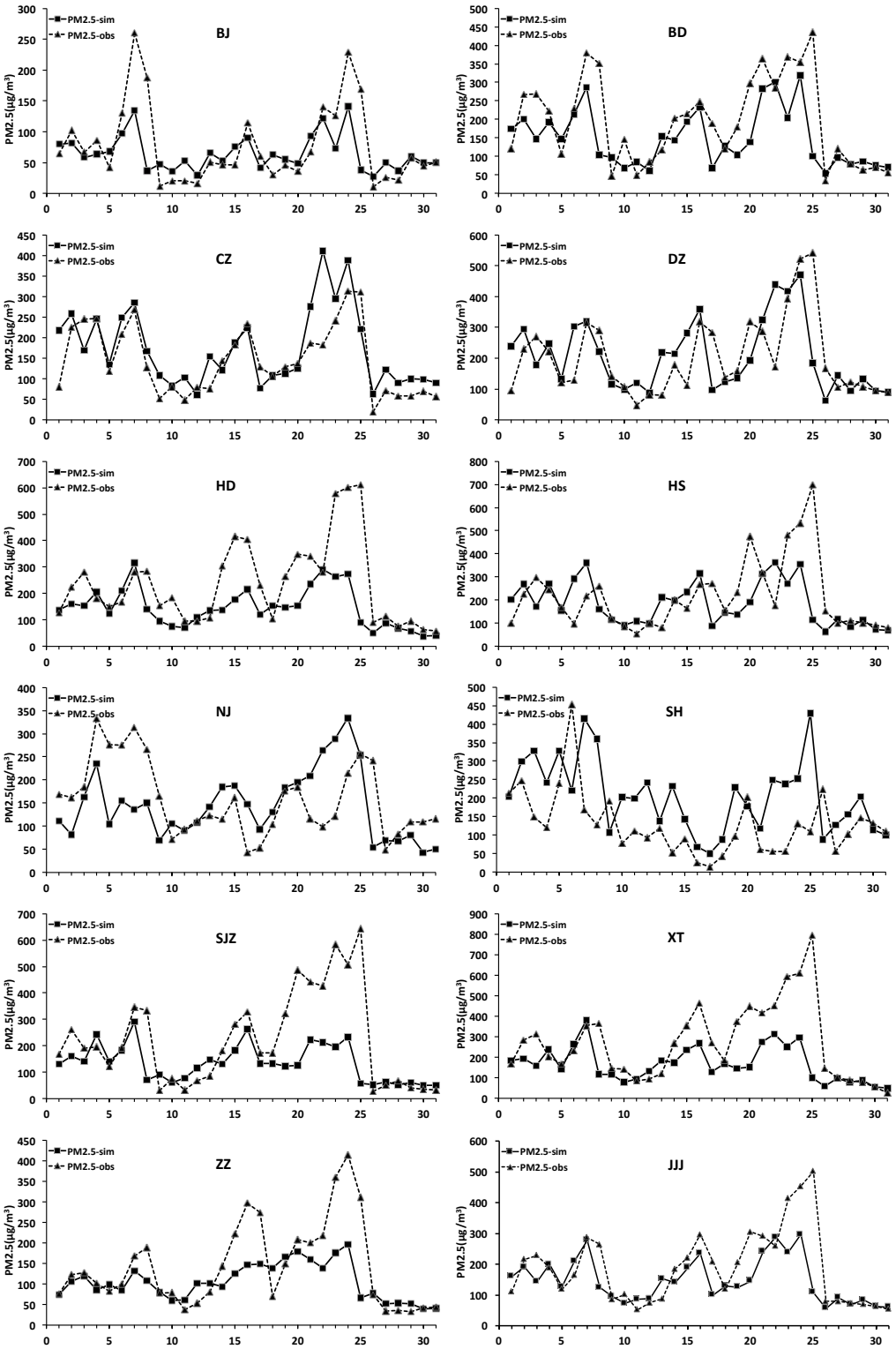

681

682 Fig. 5 (a) Horizontal wind field at 900 hPa, its vertical section at (b) 115.25°E
683 and (c) 39.375°N at 0800 UTC(1600 LT) 7 December 2013

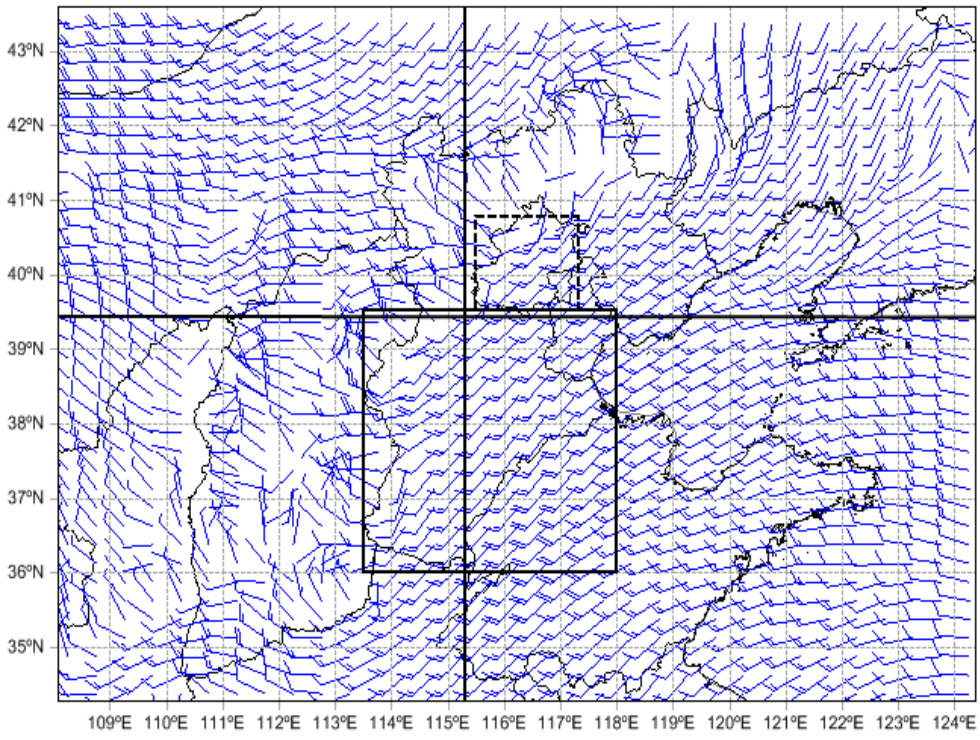

684

685 (a)

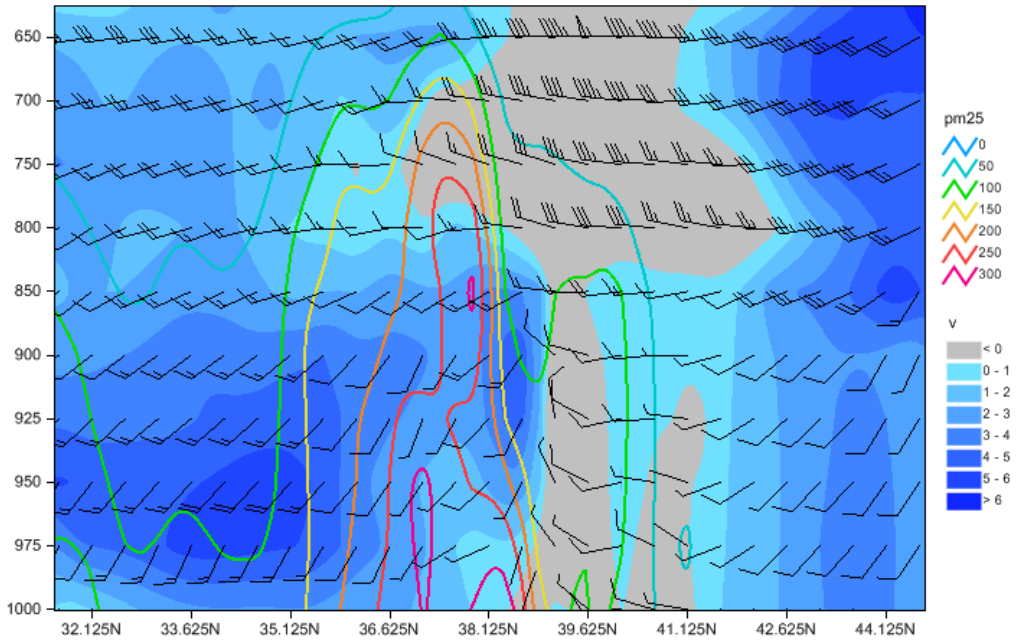

686

687 (b)

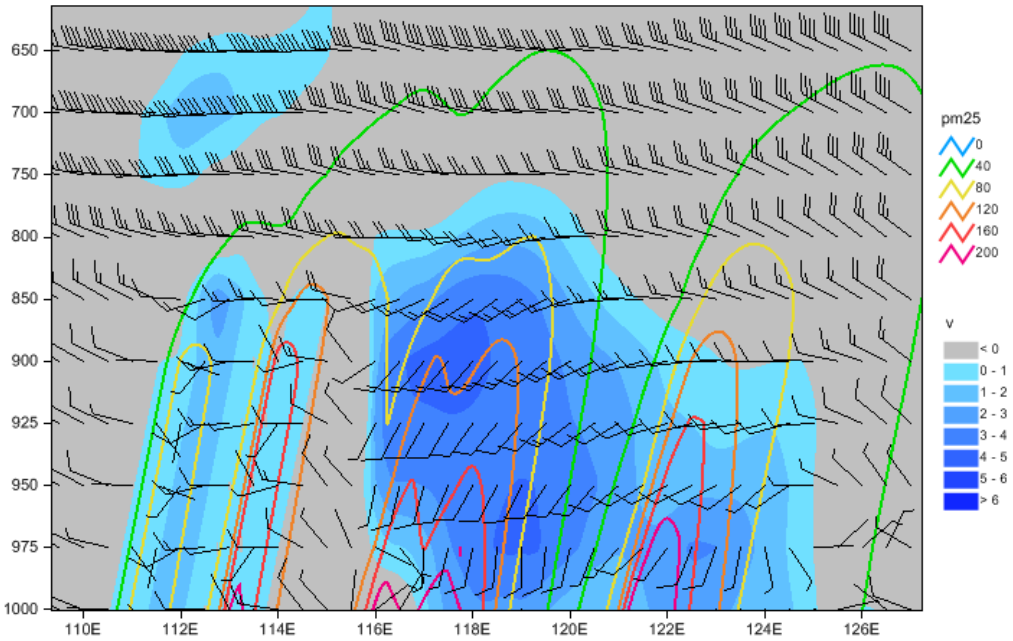
650
700
750
800
850
900
925
950
975
1000
110E
112E
114E
116E
118E
120E
122E
124E
126E
pm25
0
40
80
120
160
200
v
< 0
0 - 1
1 - 2
2 - 3
3 - 4
4 - 5
5 - 6
> 6

(c)

691 Fig. 6 Hourly variations in $PM_{2.5}$ (μg/m3) in BJ and mean southerly wind
692 speed (negative for northerly wind) for the region to the south of BJ, 1–10
693 December 2013

694

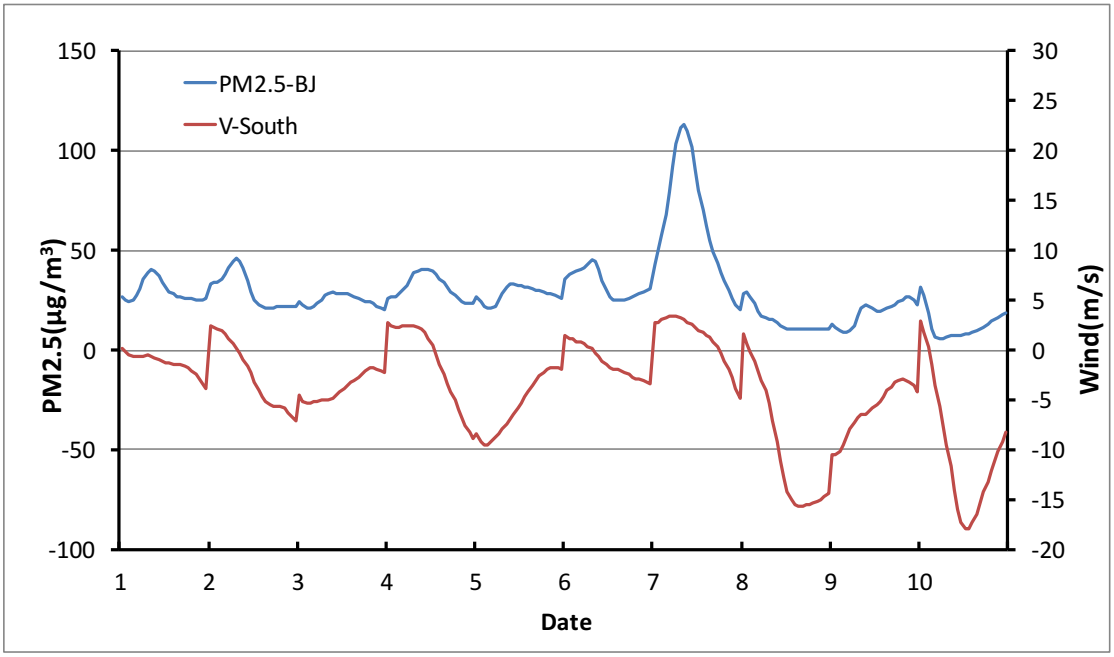

695

696 Fig. 7 Schematic diagram of pollutant transport between BJ and its
697 surrounding regions

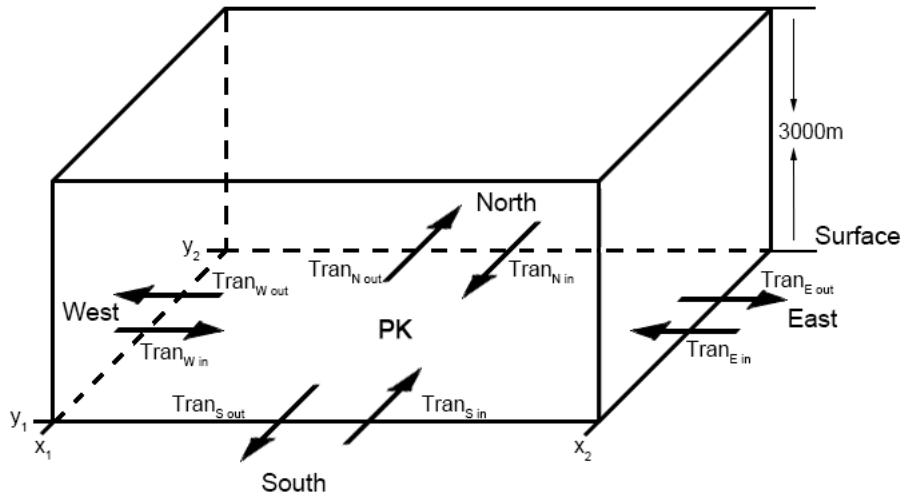

698

699 Fig. 8 $PM_{2.5}$ transport rates (kg/s) from S, N, W and E of BJ on (a) 6 and (c) 7
700 December. Total input, output and net $PM_{2.5}$ transport rate (kg/s) from BJ's
701 environs on (b) 6 and (d) 7 December

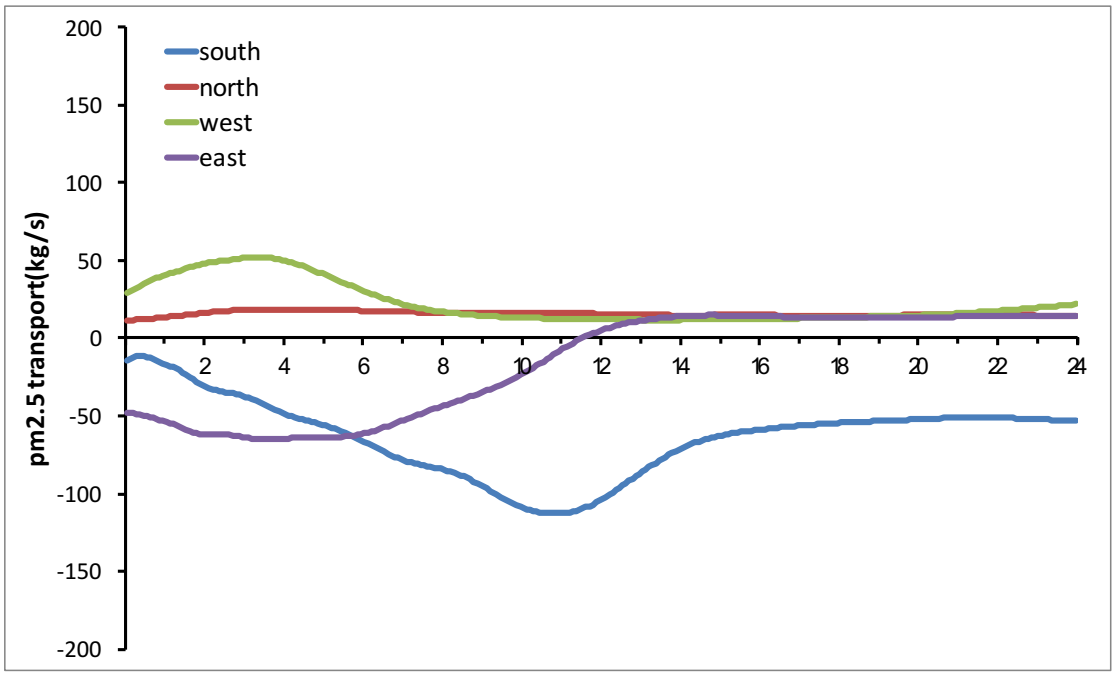

702

703 (a)

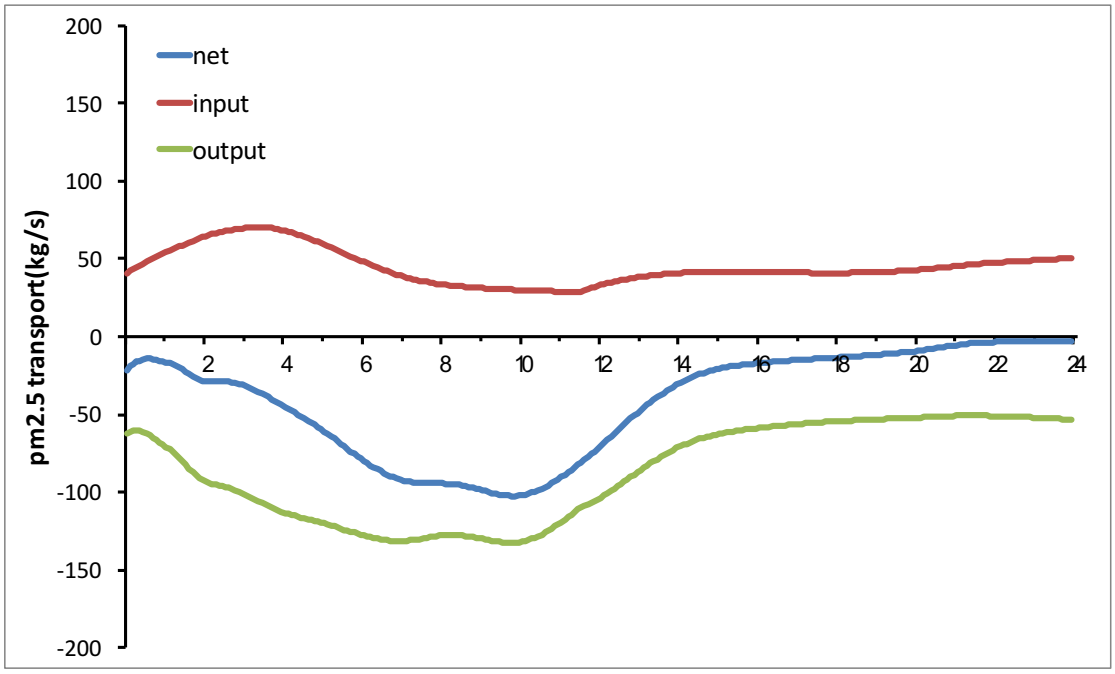

704

705 (b)

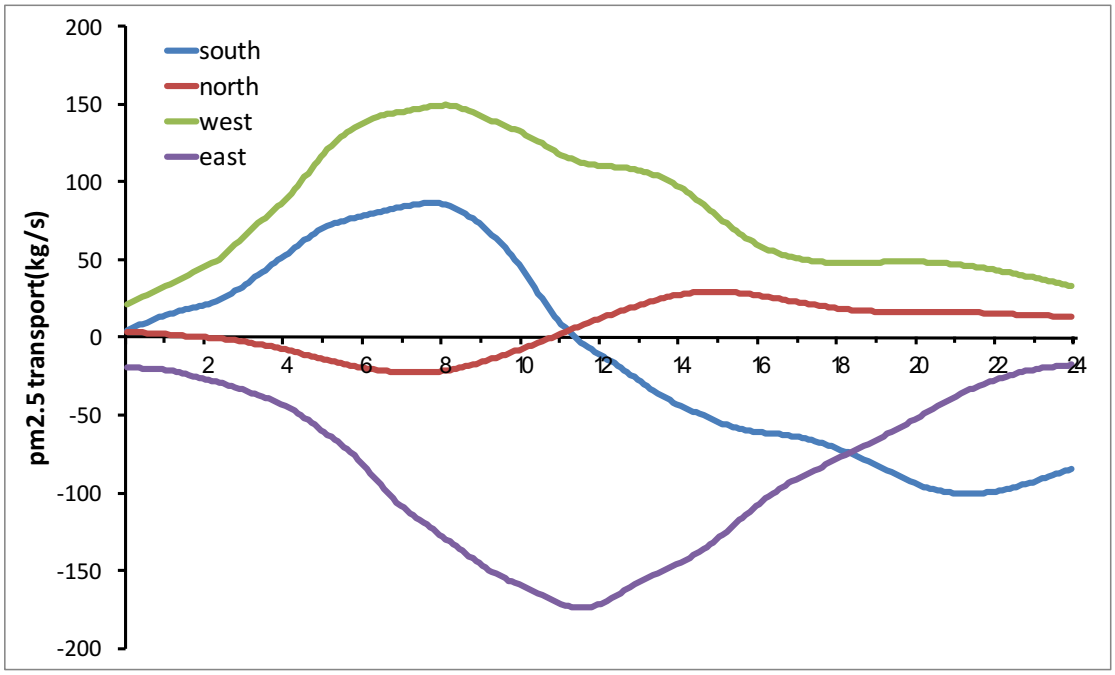
south
north
west
east
pm2.5 transport(kg/s)
200
150
100
50
0
-50
-100
-150
-200
2
4
6
8
10
12
14
16
18
20
22
24

(c)

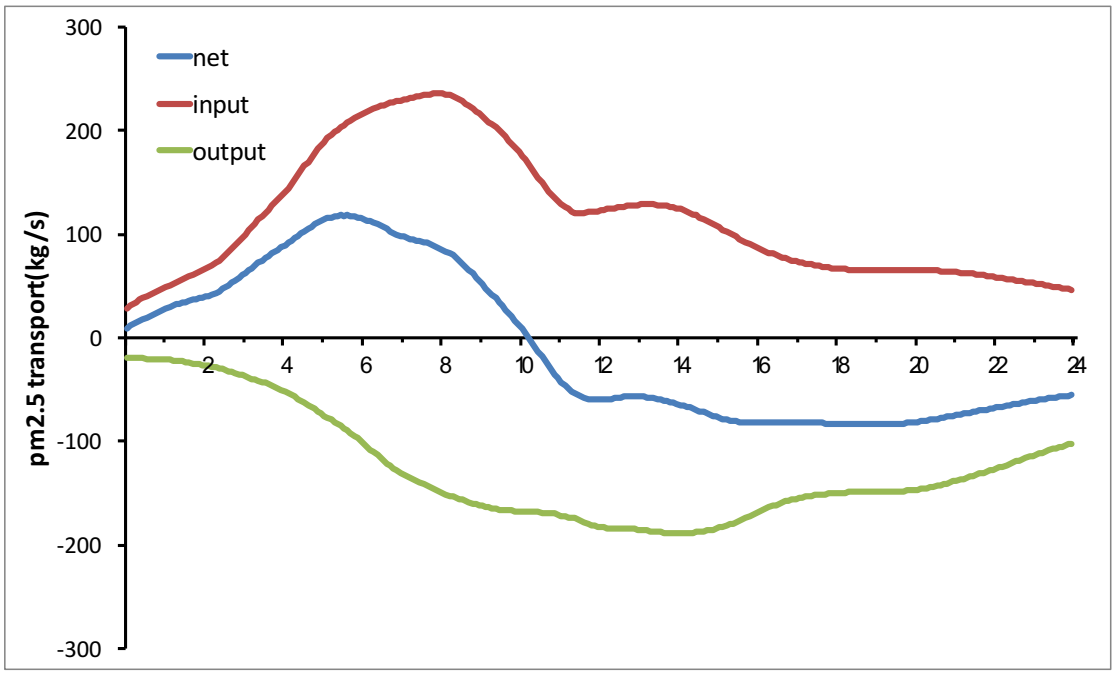
net
input
output
pm2.5 transport(kg/s)
300
200
100
0
-100
-200
-300
2
4
6
8
10
12
14
16
18
20
22
24

(d)

711 Fig. 9 Total $PM_{2.5}$ (ton) suspended in the atmosphere from the surface to 3000
712 m over the BJ area and the net hourly $PM_{2.5}$ input (ton/h) for BJ during 6–7
713 December 2013

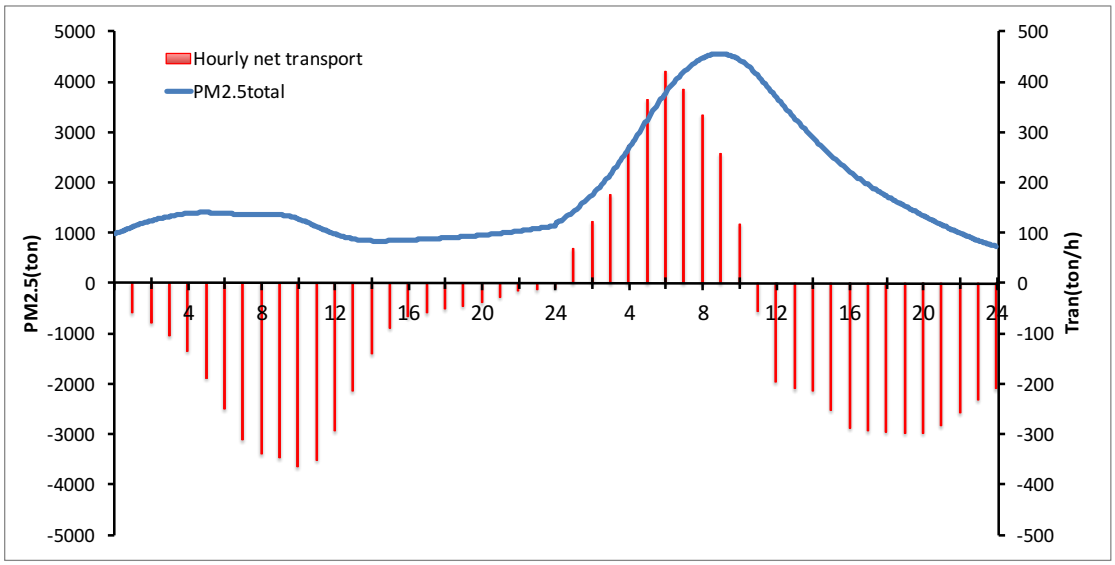

714

715

716 Fig. 10 Contribution made by net transport and local effects to $PM_{2.5}$ increases
717 in BJ, 6–7 December 2013
718

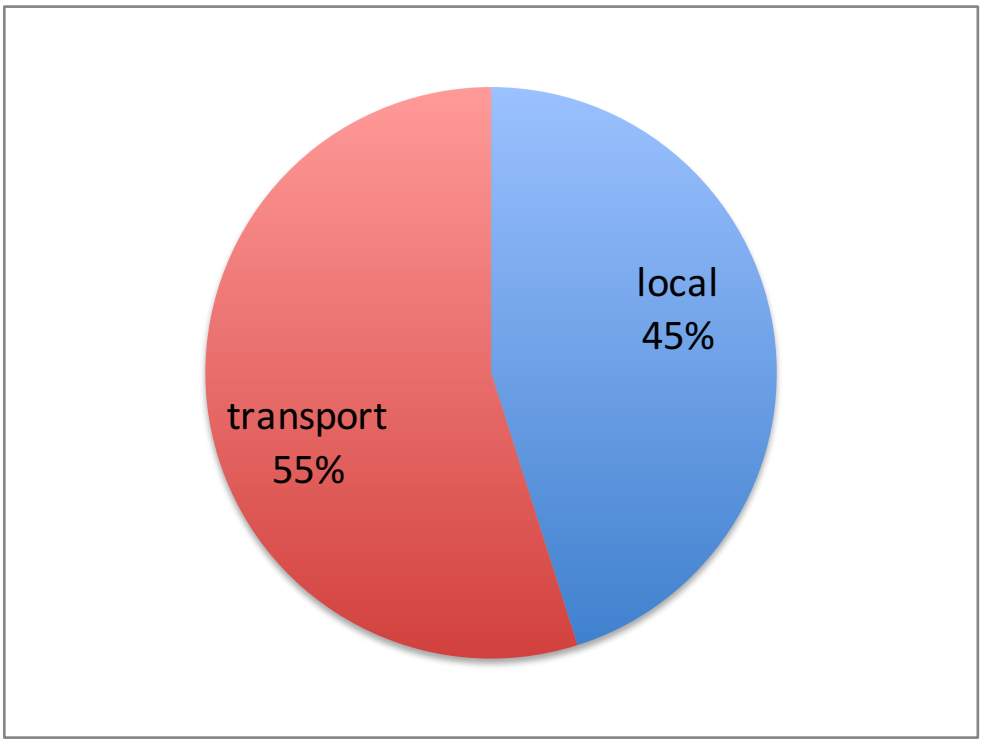

719
720